

Journal of Thermal Stresses

ISSN: 0149-5739 (Print) 1521-074X (Online) Journal homepage: https://www.tandfonline.com/loi/uths20

Effects of homogeneous and inhomogeneous heating on rotating shrink fits with annular inclusion and functionally graded hub

Tunç Apatay, Eray Arslan & Werner Mack

To cite this article: Tunç Apatay, Eray Arslan & Werner Mack (2019) Effects of homogeneous and inhomogeneous heating on rotating shrink fits with annular inclusion and functionally graded hub, Journal of Thermal Stresses, 42:11, 1458-1479, DOI: 10.1080/01495739.2019.1638856

To link to this article: https://doi.org/10.1080/01495739.2019.1638856

© 2019 The Author(s). Published with license by Taylor & Francis Group, LLC

Published online: 26 Jul 2019.

Submit your article to this journal

Article views: 548

View related articles

View Crossmark data

Full Terms & Conditions of access and use can be found at https://www.tandfonline.com/action/journalInformation?journalCode=uths20

JOURNAL OF THERMAL STRESSES
2019, VOL. 42, NO. 11, 1458–1479
https://doi.org/10.1080/01495739.2019.1638856

Taylor & Francis
Taylor & Francis Group

OPEN ACCESS Check for updates

Effects of homogeneous and inhomogeneous heating on rotating shrink fits with annular inclusion and functionally graded hub

Tunç Apatay[a], Eray Arslan[b], and Werner Mack[b]

[a]Department of Mechanical Engineering, Gazi University, Ankara, Turkey; [b]Institute of Mechanics and Mechatronics, TU Wien, Vienna, Austria

ABSTRACT

For given geometrical properties of a shrink fit, the interface pressure is decisive for reliable operation and should stay as large as possible during operation. Using an appropriate functionally graded material for the hub facilitates a less decreasing interface pressure with increasing angular speed and, moreover, substantial weight-reduction. However, temperature cycles may influence the interface pressure considerably, and if partial plastification occurs, even a permanent decrease may result. These issues are discussed by analytical means, and both homogeneous and inhomogeneous temperature fields in an initially elastic shrink fit with hollow steel inclusion and steel-aluminum FGM-hub are considered.

ARTICLE HISTORY
Received 7 June 2019
Accepted 28 June 2019

KEYWORDS
Functionally graded material; hollow cylinders; interference fit; rotation; temperature cycle

1. Introduction

Due to their beneficial properties, the interest in Functionally Graded Materials (FGMs) both in theoretical investigations and practical applications still is increasing. As is well known, a device of an FGM is manufactured by a zonation of the basic constituents of the material in such a way that the physical parameters like density, Young's modulus, coefficient of thermal expansion, etc., vary—within certain limits—continuously in a desired manner. For hollow cylinders this was discussed, e.g., in the article by Nie et al. [1]. Grading is possible in one or more direction(s), and as only two recent sample applications for both cases (in cylindrical structures) the studies by Babaei et al. [2] and Shojaeefard et al. [3] shall be quoted. Whereas basic theoretical investigations are applicable to devices of FGMs with arbitrary constituents, in general, specific results have however been given by most authors particularly for metal-ceramic composites (e.g., Haghpanah Jahromi et al. [4], Parvizi et al. [5], Seifi [6], Kalali et al. [7], and many others); a main advantage of these widely used composites is their beneficial behavior at large temperature gradients. Nevertheless, also metal-metal composites find more and more attention: For example, a steel-aluminum FGM-device offers the possibility of substantial weight-reduction while having satisfactory strength if appropriately graded for specific loads. While Sobczak and Drenchev [8] give a general survey of the main production technologies for metallic composites, a method especially

CONTACT Eray Arslan eray.arslan@tuwien.ac.at Vienna University of Technology, Institute of Mechanics and Mechatronics, Research Unit of Technical Dynamics and Vehicle System Dynamics, Getreidemarkt 9/E325-01, 1060 Vienna, Austria.

Color versions of one or more of the figures in the article can be found online at www.tandfonline.com/uths.

© 2019 The Author(s). Published with license by Taylor & Francis Group, LLC.
This is an Open Access article distributed under the terms of the Creative Commons Attribution License (http://creativecommons.org/licenses/by/4.0/), which permits unrestricted use, distribution, and reproduction in any medium, provided the original work is properly cited.

for a steel-aluminum FGM was discussed comprehensively by Nemat-Alla et al. [9]; in this method, appropriately mixed steel-aluminum powders are cold pressed and subsequently sintered.

Hence, because of the achievable weight-reduction by application of such an FGM the use of it in shrink fits was proposed by the present authors in [10–12] for the case of a solid inclusion and in [13] for a shrink fit with annular inclusion. Specifically, grading of the hub from pure steel at its inner surface to either a steel-aluminum alloy or to pure aluminum at its outer surface and a homogeneous steel-inclusion was considered. Whereas substantial saving of weight can be achieved quite generally, such type of grading proves in many cases also significantly superior to a homogeneous (steel) shrink fit if the device is subject to rotation; this is due to the less diminishing interface pressure with increasing angular speed.

Indeed, for given geometrical properties and friction at the interface between inclusion and hub (Booker and Truman [14]) solely the interface pressure is decisive for the maximum transferable load (Chu et al. [15]). Therefore, measures to keep the interface pressure (also) under operating conditions as large as possible have been a dominating subject in shrink fit studies from the very beginning. An early application-oriented basic survey on a broad class of shrink fits was given by Kollmann [16]. In his monograph, he considered elastic as well as elastic-plastic shrink fits, since the admittance of a certain degree of plastification—especially of the hub—may raise the interface pressure noticeably. Later on, many special investigations were devoted both to the commonly used thermal mounting process and the effects of various material and/or geometrical characteristics. As examples for both topics here two more recent studies shall be quoted, i.e., Doležel et al. [17] and Baykara and Güven [18], respectively. Moreover, specific design procedures were suggested, e.g., by Baldanzini [19] and Alexandrov et al. [20]; a number of further references to all of these issues can be found in these articles and also in [10, 11, 13]. Additionally, it shall be mentioned that there exist several studies on the related problems of shrink-fitted layered pressure vessels and combined shrink-fit/autofrettage procedures, see, e.g., Parker and Kendall [21], Eraslan and Akis [22], and Sharifi et al. [23].

However, in addition to the aforementioned topics in shrink fit analysis there is one further important problem that has received considerable attention, too. That is, heating during operation may influence the interface pressure considerably, and in case of plastification even after cooling a (permanent) reduction may remain. Among the first studies on this topic were the articles by Lippmann [24] and Kovács [25, 26]. In these investigations, shrink fits with hollow inclusion were considered, and the focus was on the effect of plastification by quasi-steady or homogeneous temperature distributions during the load cycles; the same applies to the more recent article by Antoni [27], who gave special attention also to the case of contact separation. In a similar way, Mack et al. [28, 29] studied a shrink fit with solid inclusion; in [24–26] and [28] shrink fits at standstill were considered. Whereas all of the aforementioned investigations were based on quasi-steady temperature fields, a rotating shrink fit with solid shaft, initially at ambient temperature and then heated and subsequently cooled from the outside of the hub was considered by Mack and Plöchl [30]. Based on an analytical solution for the transient temperature field, they studied not only the possible permanent stress-redistribution by the occurrence of a plastic zone, but also the temporary reduction of the interface pressure (in the elastic range) due to the thermal expansion of the hub.

However, in all of the above articles the case of homogeneous material(s) of inclusion and hub, respectively, was presupposed. According to this, the last-mentioned effect results—at least if the entire shrink fit consists of the same material—solely from an inhomogeneity of the temperature field. On the contrary, due to the spatial variation of the coefficient of thermal expansion, for an FGM-hub even homogeneous heating will influence the interface pressure. It was shown by the present authors that a homogeneous thermal load causes for a non-rotating shrink fit with steel/aluminum FGM-hub and solid inclusion a slightly worse performance than for one with a pure steel-hub [12], which nevertheless for moderate operating temperatures is insignificant as compared to the achievable weight-reduction and pronounced advantages at rotation [10].

Whereas in [10] an elastic shrink fit with solid inclusion loaded by both rotation and homogeneously elevated temperature was considered, in [11, 13] only rotation and in [12] only homogeneous heating was taken into account. As was shown in [13], also for the more complex case of an annular inclusion an FGM-hub may offer significant advantages; however, the influence of heating during operation remained an open question. Hence, it is the aim of the present contribution to study the combined effects of temperature fields and rotation in case of an annular inclusion and an FGM-hub. Moreover, in contrast to [10], where plane stress condition was presupposed, here "long" shrink fitted devices (e.g., Kotlan et al. [31]) under generalized plane strain are treated ([30], Haase [32]), and both homogeneous and inhomogeneous thermal loads are considered. In the latter case, heating of the inner surface of the shrink fit while keeping the outer surface at ambient temperature as well as vice versa are taken into account. Provided that the temperature at the respective surface is raised and reduced slowly, a quasi-steady treatment and hence also for an FGM-hub an analytical discussion of the entire problem is possible. Applying Tresca's yield criterion, it is found that several different elastic limit cases may occur, and exemplarily an elastic-plastic state is considered, too. A remarkable result is that heating of the inner surface increases the interface pressure, and for low angular speeds, it even may become larger than at standstill. As a matter of course, comparisons with homogeneous shrink fits are also provided, and both cases where use of an FGM-hub offers advantages also for thermally loaded shrink fits and cases where a homogeneous hub is preferable are discussed.

As a supplement, some hints to more recent articles on related topics shall be given, too: A homogeneous rotating hollow shaft subject to a positive temperature gradient was treated by Eraslan et al. [33] and the analogous case of a solid shaft heated and cooled from its outside by Arslan et al. [34], asymmetrical surface heating of FGM/multilayered hollow cylinders was studied by Ootao and Tanigawa [35] and Ootao and Ishihara [36], thick walled tubes subject to periodic surface temperatures were investigated by Apatay and Eraslan [37], and a thermal shock at the inner surface of a hollow FGM-cylinder governed by generalized thermoelasticity has been the subject of the article by Wang et al. [38].

The article is organized as follows: First, the mathematical statement of the problem and the (mechanical) governing equations are given. Subsequently, the occurring temperature distributions are derived. Based thereon, the interface pressure and the elastic limits are discussed, and also an elastic-plastic case is studied. Finally, the results are summarized in some concluding remarks.

2. Statement of the problem

The subject of the study is a shrink fit compounded of a homogeneous hollow cylindrical inclusion $(a \le r \le b)$ and an FGM-hub $(b \le r \le c)$, see Figure 1. The inner and outer surfaces are presumed to be stress-free, i.e.,

$$r = a: \quad \sigma_{r,i} = 0, \tag{1}$$

$$r = c: \quad \sigma_{r,h} = 0; \tag{2}$$

throughout the article, the indices i and h denote the inclusion and the hub, respectively, and standard cylindrical coordinates are employed. For a shrink fit with a hub with an axial length L about equal to (or larger than) the diameter of the inclusion a treatment as a (generalized) plane strain problem is appropriate. Hence, the condition of vanishing axial force on any section,

$$2\pi\int_a^b \sigma_{z,i}(r)rdr + 2\pi\int_b^c \sigma_{z,h}(r)rdr = 0, \tag{3}$$

determines the spatially constant axial strain $\epsilon_0 = \epsilon_z(\omega, T)$; there, ω means the angular speed and T the difference of current and ambient temperature. At the interface the radial stress must be continuous, i.e.,

$$r = b: \quad \sigma_{r,i} = \sigma_{r,h}, \tag{4}$$

and the radial displacements u_j must comply with the relation

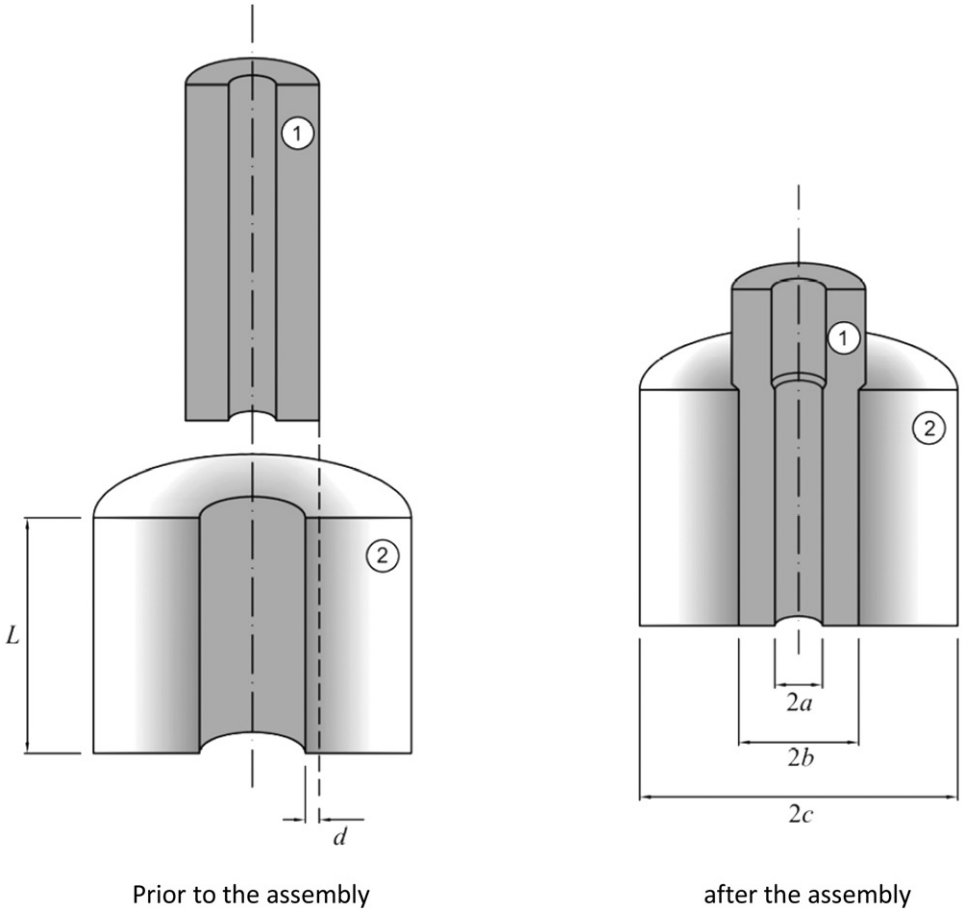


Figure 1. Sketch of the shrink fit; ① homogeneous annular inclusion and ② FGM-hub.

$$r = b: \quad u_h - u_i = d \tag{5}$$

where d denotes the interference.

Furthermore, it is presupposed that ω is only slowly varying and that the device has reached its constant operating angular speed prior to the occurrence of heating. The elastic limit is presumed to be determined by Tresca's yield criterion (for details see, e.g., the textbook by Chen and Han [39]).

3. Governing equations

The governing equations for the FGM under consideration without heating were given already in [13]; here, they are supplemented with the appropriate temperature-terms, and the derivations will be sketched only.

Allowing for a radially variable density ρ, the equation of motion for the radial direction reads

$$\frac{d(r\sigma_r)}{dr} - \sigma_\theta = -\rho(r)\omega^2 r^2, \tag{6}$$

and within the geometrically linear theory the relations

$$\epsilon_r = \frac{du}{dr}, \quad \epsilon_\theta = \frac{u}{r} \tag{7}$$

hold. Taking also a variation of Young's modulus E and the coefficient of thermal expansion α into account, the generalized Hooke's law reads

$$\epsilon_r = \frac{1}{E(r)}[\sigma_r - \nu(\sigma_\theta + \sigma_z)] + \alpha(r)T(r) + \epsilon_r^p, \tag{8}$$

$$\epsilon_\theta = \frac{1}{E(r)}[\sigma_\theta - \nu(\sigma_r + \sigma_z)] + \alpha(r)T(r) + \epsilon_\theta^p, \tag{9}$$

$$\epsilon_z = \epsilon_0 = \frac{1}{E(r)}[\sigma_z - \nu(\sigma_r + \sigma_\theta)] + \alpha(r)T(r) + \epsilon_z^p \tag{10}$$

where ϵ_j^p denotes a plastic strain component; as frequently presumed for cylindrical FGM-devices, Poisson's ratio ν is considered as constant (see, e.g., [13], Sharma and Yadav [40], Nejad and Fatehi [41]). As a matter of course, in a virgin elastic material $\epsilon_j^p = 0$.

For the FGM-hub, it is presupposed that E, α, and ρ—and also the uniaxial yield limit σ_y and the thermal conductivity k—depend on the radial coordinate by a power law [13, 41]. Moreover, an effective material property Pr_{eff} is obtained by the rule of mixture,

$$\mathrm{Pr}_{eff}(r) = \mathrm{Pr}_1 V_1(r) + \mathrm{Pr}_2 V_2(r) \tag{11}$$

where V_j ($j = 1, 2$) means the volume fraction of constituent j with property Pr_j. In the present study, it is presumed that the material at the inner surface of the hub is pure FGM-constituent s, the same material as used for the homogeneous inclusion; hence, $V_s(b) = 1$. Denoting the other FGM-constituent by l, for the hub there holds

$$V_l(r) = 1 - V_s(r). \tag{12}$$

Now, it is postulated that V_s depends on r by

$$V_s(r) = \frac{E_s\left(\frac{r}{b}\right)^m - E_l}{E_s - E_l} \tag{13}$$

where m means the grading index. Whereas this relation is a particular one, indeed, it facilitates both to reasonably approximate by a proper choice of m also several other types of grading, and—most significant—to analytically discuss the problem under consideration. Thus, from Eqs. (11)–(13) one obtains for Young's modulus the elementary relation

$$E(r) = E_s\left(\frac{r}{b}\right)^m \tag{14}$$

which corresponds to the upper bound of $E(r)$ in the homogenization theory of composites, see Nakamura et al. [42]. For the other material parameters then there follows

$$\mathrm{Pr}_{eff}(r) = A_{\mathrm{Pr}}\left(\frac{r}{b}\right)^m + B_{\mathrm{Pr}} \tag{15}$$

where

$$A_{\mathrm{Pr}} = \frac{E_s(\mathrm{Pr}_s - \mathrm{Pr}_l)}{E_s - E_l}, \quad B_{\mathrm{Pr}} = \frac{E_s\mathrm{Pr}_l - E_l\mathrm{Pr}_s}{E_s - E_l}, \tag{16}$$

and $\mathrm{Pr} = \alpha$, ρ, σ_y, and k, respectively.

4. Elastic behavior

Starting from the equation of motion (6) and setting $\epsilon_j^p = 0$ in Eqs. (8)–(10), one first derives from the governing equations a differential equation for the radial displacement,

$$\begin{aligned} & r^{1+m}u'' + (1+m)r^m u' - \frac{1-\nu(1+m)}{1-\nu} r^{-1+m} u \\ & = \frac{1+\nu}{1-\nu}\left[mr^m \left(2A_\alpha \frac{r^m}{b^m} + B_\alpha \right) T(r) + r^{1+m} \left(A_\alpha \frac{r^m}{b^m} + B_\alpha \right) T'(r) \right. \\ & \left. - \frac{1-2\nu}{E_s}(A_\rho r^m + B_\rho b^m)\omega^2 r^2 \right] - \frac{m\nu r^m}{1-\nu}\epsilon_0 \end{aligned} \tag{17}$$

where a prime means a derivative with respect to r. Its solution is

$$\begin{aligned} u = {} & C_1 r^{(-m-M)/2} + C_2 r^{(-m+M)/2} - r\nu\epsilon_0 - 4\left[\frac{A_\rho r^m}{(6+m)^2 - M^2} + \frac{B_\rho b^m}{(6-m)^2 - M^2} \right] \\ & \times \frac{(1+\nu)(1-2\nu)r^{3-m}}{E_s(1-\nu)}\omega^2 + \frac{(1+\nu)r^{(-m-M)/2}}{2b^m M(1-\nu)} \\ & \times \left\{ (2-m+M)\left[\int A_\alpha r^{(3m+M)/2} T(r)dr + \int B_\alpha b^m r^{(m+M)/2} T(r)dr \right] \right. \\ & \left. - (2-m-M)r^M \left[\int A_\alpha r^{(3m-M)/2} T(r)dr + \int B_\alpha b^m r^{(m-M)/2} T(r)dr \right] \right\} \end{aligned} \tag{18}$$

with the constants of integration C_j and the abbreviation

$$M = \sqrt{4 + m^2 - \frac{4m\nu}{1-\nu}}. \tag{19}$$

Based thereon, σ_r and σ_θ are obtained,

$$\begin{aligned} \sigma_r = {} & \frac{-E_s b^{-m}}{2(1+\nu)(1-2\nu)} \left\{ C_1[m+M-(2+m+M)\nu] r^{(m-M-2)/2} + C_2[m-M-(2+m-M)\nu] \right. \\ & \left. \times r^{(m+M-2)/2} \right\} - \frac{4r^2\omega^2}{1-\nu} \left\{ \frac{A_\rho r^m b^{-m}(3-2\nu)}{(6+m)^2 - M^2} + \frac{B_\rho[3-m(1-\nu)-2\nu]}{(6-m)^2 - M^2} \right\} \\ & + \frac{E_s r^{(m-M-2)/2} b^{-2m}}{4M(1-\nu)(1-2\nu)} \left\{ r^M (m+M-2)[-m+M+(2+m-M)\nu] \right. \\ & \times \left[A_\alpha \int T(r) r^{(3m-M)/2} dr + b^m B_\alpha \int T(r) r^{(m-M)/2} dr \right] - (m-M-2) \\ & \times [-m-M+(2+m+M)\nu] \left[A_\alpha \int T(r) r^{(3m+M)/2} dr \right. \\ & \left. \left. + b^m B_\alpha \int T(r) r^{(m+M)/2} dr \right] \right\}, \end{aligned} \tag{20}$$

$$\sigma_\theta = \frac{E_s b^{-m}}{2(1+\nu)(1-2\nu)}\Big\{C_1[2-(2+m+M)\nu]r^{(m-M-2)/2} + C_2[2-(2+m-M)\nu] \times r^{(m+M-2)/2}\Big\} - \frac{4r^2\omega^2}{1-\nu}\left\{\frac{A_\rho r^m b^{-m}(1+2\nu)}{(6+m)^2-M^2} + \frac{B_\rho[1+(2-m)\nu]}{(6-m)^2-M^2}\right\} - \frac{E_s b^{-2m} r^m (r^m A_\alpha + b^m B_\alpha)}{1-\nu}T(r) + \frac{E_s b^{-2m} r^{(m-M-2)/2}}{4M(1-\nu)(1-2\nu)}\Big\{r^M(m+M-2) \times [2-(2+m-M)\nu]\left[A_\alpha\int T(r)r^{(3m-M)/2}dr + b^m B_\alpha\int T(r)r^{(m-M)/2}dr\right] - (m-M-2)[2-(2+m+M)\nu]\left[A_\alpha\int T(r)r^{(3m+M)/2}dr + b^m B_\alpha\int T(r)r^{(m+M)/2}dr\right]\Big\}, \tag{21}$$

respectively, and σ_z then follows from Eq. (10); for $m = 0$, these relations also hold for the homogeneous inclusion.

Here, however a remark is appropriate. For a few discrete values of m the above formulae are not directly applicable: This can be seen, e.g., from the factor of A_ρ, which excludes a grading index of $m = -8(1-\nu)/(3-2\nu)$; other ones come from the factors of B_ρ and the temperature terms, respectively. Nevertheless, these mathematically singular cases can be approximated numerically with arbitrary accuracy by choosing some m close to the respective values (or are not relevant here at all) and are not treated severally; the same applies analogously in the plastic range.

5. Plastic behavior with $\sigma_\theta(r) > \sigma_z(r) > \sigma_r(r)$

As will be shown below, in case of partial plastification of the hub a commonly occurring Tresca regime is governed by the relation (compare also [30])

$$\sigma_{Tresca}(r) = \sigma_y(r) = \sigma_\theta(r) - \sigma_r(r). \tag{22}$$

Insertion of Eq. (22) into the equation of motion (6), taking Eq. (15) into account, and integration give

$$\sigma_r = \left(\frac{r}{b}\right)^m \frac{A_{\sigma_y}}{m} + B_{\sigma_y}\ln r - r^2\omega^2\left[\left(\frac{r}{b}\right)^m \frac{A_\rho}{2+m} + \frac{B_\rho}{2}\right] + C_3 \tag{23}$$

with the constant of integration C_3, and σ_θ then comes from relation (22), too. According to the associated flow rule there follows for the plastic strain increments $d\epsilon_\theta^p = -d\epsilon_r^p, d\epsilon_z^p = 0$, and hence in case of monotonously increasing load

$$\epsilon_\theta^p = -\epsilon_r^p, \quad \epsilon_z^p = 0. \tag{24}$$

Because of the latter relation, the axial strain consists of an elastic and a thermal part only, and Eq. (10) yields the same expression for σ_z as in the previous case.

From plastic incompressibility (24) it follows also that the dilatation is governed by the generalized Hooke's law, and taking the geometric relations (7) into account, a differential equation for the radial displacement is obtained, i.e.,

$$\begin{aligned}\frac{du}{dr}+\frac{u}{r}&=2C_3\left(\frac{r}{b}\right)^{-m}\frac{(1+\nu)(1-2\nu)}{E_s}-2\nu\epsilon_0\\&\quad-r^2\left(\frac{r}{b}\right)^{-m}\frac{(1+\nu)(1-2\nu)}{E_s(2+m)}\left[2A_\rho\left(\frac{r}{b}\right)^m+B_\rho(2+m)\right]\omega^2\\&\quad+\left(\frac{r}{b}\right)^{-m}\frac{(1+\nu)(1-2\nu)}{E_s m}\left[(2+m)\left(\frac{r}{b}\right)^m A_{\sigma_y}+mB_{\sigma_y}(1+2\ln r)\right]\\&\quad+2(1+\nu)\left[A_\alpha\left(\frac{r}{b}\right)^m+B_\alpha\right]T(r).\end{aligned}\tag{25}$$

Its solution reads

$$\begin{aligned}u&=2r\left(\frac{r}{b}\right)^{-m}\frac{(1+\nu)(1-2\nu)}{(2-m)E_s}C_3+\frac{C_4}{r}-r\nu\epsilon_0\\&\quad-\frac{(1+\nu)(1-2\nu)}{2E_s}\left[\frac{A_\rho}{2+m}+\frac{2B_\rho}{4-m}\left(\frac{r}{b}\right)^{-m}\right]r^3\omega^2\\&\quad+r\frac{(1+\nu)(1-2\nu)}{2E_s}\left\{\frac{A_{\sigma_y}(2+m)}{m}-\frac{2B_{\sigma_y}[m-2(2-m)\ln r]}{(2-m)^2}\left(\frac{r}{b}\right)^{-m}\right\}\\&\quad+\frac{2(1+\nu)}{r}\int r\left[A_\alpha\left(\frac{r}{b}\right)^m+B_\alpha\right]T(r)dr\end{aligned}\tag{26}$$

with the further constant of integration C_4.

Finally, the circumferential plastic strain component is found as the difference of the total circumferential strain and its elastic and thermal parts, so that, taking also Eq. (24) into account,

$$\begin{aligned}\epsilon_\theta^p=-\epsilon_r^p&=\left(\frac{r}{b}\right)^{-m}\frac{(1+\nu)(1-2\nu)}{(2-m)E_s}mC_3+\frac{C_4}{r^2}+\left(\frac{r}{b}\right)^{-m}\frac{\omega^2r^2(1+\nu)(1-2\nu)}{2E_s(4-m)(2+m)}\\&\quad\times\left[A_\rho(4-m)\left(\frac{r}{b}\right)^m+B_\rho(4-m^2)\right]-\left(\frac{r}{b}\right)^{-m}\frac{(1+\nu)}{2(2-m)^2E_s}\left\{A_{\sigma_y}(2-m)^2\left(\frac{r}{b}\right)^m\right.\\&\quad\left.-2B_{\sigma_y}\left\{m[3-m(1-\nu)-2\nu]-4(1-\nu)+m(2-m)(1-2\nu)\ln r\right\}\right\}\\&\quad+\frac{2(1+\nu)}{r^2}\int r\left[A_\alpha\left(\frac{r}{b}\right)^m+B_\alpha\right]T(r)dr-(1+\nu)\left[A_\alpha\left(\frac{r}{b}\right)^m+B_\alpha\right]T(r).\end{aligned}\tag{27}$$

6. Temperature field

Allowing for a radially variable thermal conductivity k, the governing equation of heat conduction reads (e.g., Jabbari et al. [43])

$$\frac{1}{r}\frac{d}{dr}\left[k(r)r\frac{dT(r)}{dr}\right]=0;\tag{28}$$

as already mentioned in the Introduction, the presupposition of slowly changing surface temperature(s) justifies a quasi-steady treatment of the problem. Moreover, the investigation is based on perfect thermal contact of inclusion and hub. Hence, the temperature distributions in the shrink fit can be calculated like those in a single hollow cylinder with a dependence of k on the radial coordinate according to

$$k(r) = k_s = \text{const. for } a \le r \le b, \quad k(r) = A_k\left(\frac{r}{b}\right)^m + B_k \text{ for } b \le r \le c \tag{29}$$

and the (thermal) boundary conditions

$$T(a) = T_a, \quad T(c) = T_c. \tag{30}$$

The general solution of Eq. (28) reads

$$T(r) = \int \frac{D_1 dr}{rk(r)} + D_2 \tag{31}$$

with the constants of integration D_1 and D_2. Applying the boundary conditions (30), there follows

$$D_1 = \frac{T_c - T_a}{\int_a^c \frac{dr}{rk(r)}}, \quad D_2 = T_a, \tag{32}$$

and thus the temperature field as

$$T(r) = \frac{T_c - T_a}{\int_a^c \frac{dr}{rk(r)}} \int_a^r \frac{dr}{rk(r)} + T_a. \tag{33}$$

For the FGM power law for $k(r)$ under consideration the integrals appearing in this equation can be given in closed form (compare also Haskul et al. [44]), i.e.,

$$\int_a^r \frac{dr}{rk(r)} = \frac{1}{k_s}\ln\frac{r}{a} \qquad \text{for } a \le r \le b, \tag{34}$$

$$\int_b^r \frac{dr}{rk(r)} = \frac{m\ln\frac{r}{b} + \ln(A_k + B_k) - \ln\left[A_k\left(\frac{r}{b}\right)^m + B_k\right]}{mB_k} \qquad \text{for } b \le r \le c; \tag{35}$$

as a matter of course, for $b \le r \le c$ the integral from a to r (or c) in Eq. (33) is found as the sum of the respective sub-integrals. Hence, for given values of T_a and T_c, with the above presuppositions the temperature distributions in the shrink fit are determined by Eqs. (33)–(35) and thus by analytical equations; for comparison, the unsteady temperature distribution merely in a single hollow cylinder with uniform exponential FGM-law throughout it and subject to a (fast) linear surface temperature increase, e.g., required an involved Laplace transform and power series solution (Shao and Ma [45]). However, although at least some of the integrals containing the temperature in the stress-equations could be given in closed form, too, the expressions—containing hypergeometric functions—are quite intricate, and therefore all of these integrals are evaluated numerically.

In the following, it is presumed that either both surface temperatures are uniformly varied—leading to a homogeneous temperature distribution—or that one of the surfaces is kept at ambient temperature.

7. Interface pressure and elastic limits

As long as the entire shrink fit behaves elastically, to calculate the stress distributions the four constants of integration C_{1i}, C_{2i}, C_{1h}, and C_{2h}, and the axial strain have to be determined. This is accomplished by numerically solving the system of equations given by conditions (1)–(5). However, as already mentioned, under certain circumstances a plastic region may emerge, e.g., at the inner edge of the hub. Then, in addition to the aforementioned unknowns the two further constants of integration C_3 and C_4 and the plastic-elastic border radius r_p must be found. In this

case, conditions (1)–(5) have to be supplemented with three further ones at the radius r_p (which also is determined by these conditions): as was discussed by Gamer et al. [46], the continuity of three properly chosen quantities at the boundary of a Tresca region, e.g., of the radial and circumferential stress, respectively, and of the radial displacement, implies the continuity of all the other ones. (By the way, if axial plastic deformation does not occur, for Tresca-based cylindrically symmetric elastic-plastic problems an alternative treatment based on a universal expression for $u(r)$ is possible, see Gamer [47].)

For the numerical calculations, it is convenient to introduce the following non-dimensional quantities:

$$\bar{k} = k/k_s,\ \bar{r} = r/b,\ \bar{u} = uE_s/\left(b\sigma_{ys}\right),\ \bar{E} = E/E_s,\ \bar{T} = E_s\alpha_s T/\sigma_{ys}, \tag{36}$$

$$\bar{\alpha} = \alpha/\alpha_s,\ \bar{\epsilon} = \epsilon E_s/\sigma_{ys},\ \bar{\rho} = \rho/\rho_s,\ \bar{\sigma}_i = \sigma_i/\sigma_{ys},\ \Omega = \omega b\sqrt{\rho_s/\sigma_{ys}}. \tag{37}$$

The volume fraction of constituent s then reads

$$V_s(\bar{r}) = \frac{\bar{r}^m - \bar{E}_l}{1 - \bar{E}_l}. \tag{38}$$

Moreover, to assess the weight reduction by use of the FGM, the weight of the hub is non-dimensionalized by the weight of a homogeneous hub of constituent s, which yields

$$\bar{W}_h = \frac{2\int_b^c \rho(r)rdr}{\rho_s(c^2 - b^2)} = \frac{c^2\left[2A_\rho\left(\frac{c}{b}\right)^m + B_\rho(2+m)\right] - b^2[2A_\rho + B_\rho(2+m)]}{\rho_s(c^2 - b^2)(2+m)}. \tag{39}$$

An important remark is the following one: The admissible value of the grading index is limited by that just leading to zero volume fraction of constituent s at the outer (cylindrical) surface of the hub. Hence, from Eq. (38) one obtains the extremum value

$$m_{ext} = \ln(\bar{E}_l)/\ln(\bar{c}). \tag{40}$$

Obviously, m_{ext} depends on the geometric ratio c/b and also on the ratio of Young's moduli of the FGM-constituents; since here particularly a hub with grading from steel (s) at $r = b$ to either a steel-aluminum alloy or to pure aluminum (l) at $r = c$ is considered, and $E_l < E_s$, there follows $m_{ext} \leq m < 0$ (note that for $m \to 0$ a homogeneous hub is recovered).

As is well known, the values of many physical parameters of steel may lie within a comparatively wide range and depend on the specific steel-type (e.g., Hahn and Özişik [48]); in the present investigation, the numerical results are based on

$$\bar{k}_l = 4.44, \quad \bar{E}_l = 0.35, \quad \bar{\alpha}_l = 1.40, \quad \bar{\rho}_l = 0.35, \quad \bar{\sigma}_{yl} = 0.15, \tag{41}$$

and $\nu_l = \nu_s = 0.3$ is presupposed.

Prior to the discussion of the consequences of homogeneous and inhomogeneous heating of the shrink fit, as an example the dependencies of the properties of the FGM-hub on the radial coordinate for the parameter values in Eq. (41), $\bar{c} = c/b = 5.0$, and $m = m_{ext}$ are depicted in Figure 2a and b. Furthermore, in Figure 2c the dependence of $\bar{W}_h$ on the grading index is shown. As one can see, for $\bar{c} = 5.0$ more than halving the weight of a homogeneous steel hub is possible; for comparison, also the analogous curve for $\bar{c} = 2.5$ is given. Obviously, the achievable relative weight reduction increases both with increasing width of the hub and (absolute) value of the grading index.

In addition, examples of the occurring temperature distributions for both a heated inner and outer (cylindrical) surface of the shrink fit, respectively, are presented in Figure 3; there, a thick-walled inclusion with $\bar{a} = a/b = 0.25$ and the cases of $\bar{c} = 2.5$ and $\bar{c} = 5.0$, respectively, are considered.

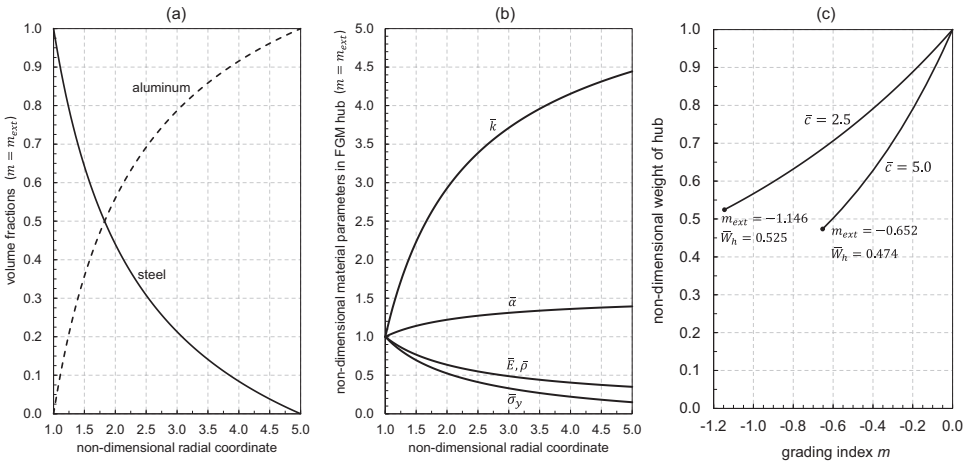


Figure 2. (a) Volume fractions; (b) Young's modulus, density, uniaxial yield limit, and thermal properties (for $m = m_{ext}$) in the hub vs. non-dimensional radius; (c) non-dimensional weight of the hub vs. grading index.

7.1. Elastic states

First, Figure 4 shows for a shrink fit with a thick-walled inclusion ($\bar{a} = 0.25$) as well as with a medium-walled inclusion ($\bar{a} = 0.5$) and a hub with $\bar{c} = 5.0$ the evolution of the interface pressure $\bar{p} := -\bar{\sigma}_r(1)$ with increasing angular speed in the absence of a temperature field. Here and in the following, a wide hub is considered, as then the effects to be discussed become particularly pronounced and clearly visible. Since at the design of a shrink fit usually the initial interface pressure is a prescribed quantity, in both cases $\bar{p}(\Omega = 0,\ \bar{T} = 0) = 0.35$ is chosen (which requires appropriately determined different values of the interference, of course). One observes that here an FGM-hub shows significant advantages as compared to a homogeneous one: For example, at the quite high angular speed of $\Omega = 0.15$ (see Appendix), the interface pressure is for the considered FGM-hub and $\bar{a} = 0.25$ about 75% higher and for $\bar{a} = 0.5$ about 45% higher than for a homogeneous hub. (It shall be mentioned that for elastic shrink fits with thin-walled inclusions quite generally only moderate values of $\bar{p}$ can be realized [13], and hence such shrink fits will not be considered here).

Hence, it is interesting to see whether an FGM-hub still shows benefits in case of different types of heating; subsequently, always the previously chosen initial value of $\bar{p} = 0.35$ at standstill and ambient temperature is chosen. Figure 5a and b provide for the thick-walled inclusion with $\bar{a} = 0.25$ and heated inner surface a comparison of the interface pressure for a homogeneous and a maximum graded FGM-hub, respectively, at different angular speeds. Moreover, the elastic limits (dashed lines) and the respective Tresca regimes at the onset of plastification are shown; note that yielding may start at quite different locations! Nevertheless, primarily one notices that irrespective of the hub-material the occurring negative temperature gradients lead to an increase of $\bar{p}$ at all angular speeds. Furthermore, it can be seen that for a homogeneous hub this increase is more pronounced and that generally a higher operating temperature is possible within the elastic range. Thus, at first glance this might seem to contradict using an FGM-hub (at least if the achievable weight-reduction is disregarded). However, in Figure 5c the respective lines for a homogeneous hub (red) and the FGM-hub under consideration (blue) are contrasted directly, and from this figure the conditions under which the FGM-hub proves advantageous are clearly visible. Whereas at standstill the interface pressure is higher for a homogeneous hub than for the FGM-hub at all values of $\bar{T}_a > 0$ (admissible for elastic behavior), the reverse holds true already for $\Omega = 0.1$, and this effect becomes even more pronounced at higher angular speeds. Indeed, at

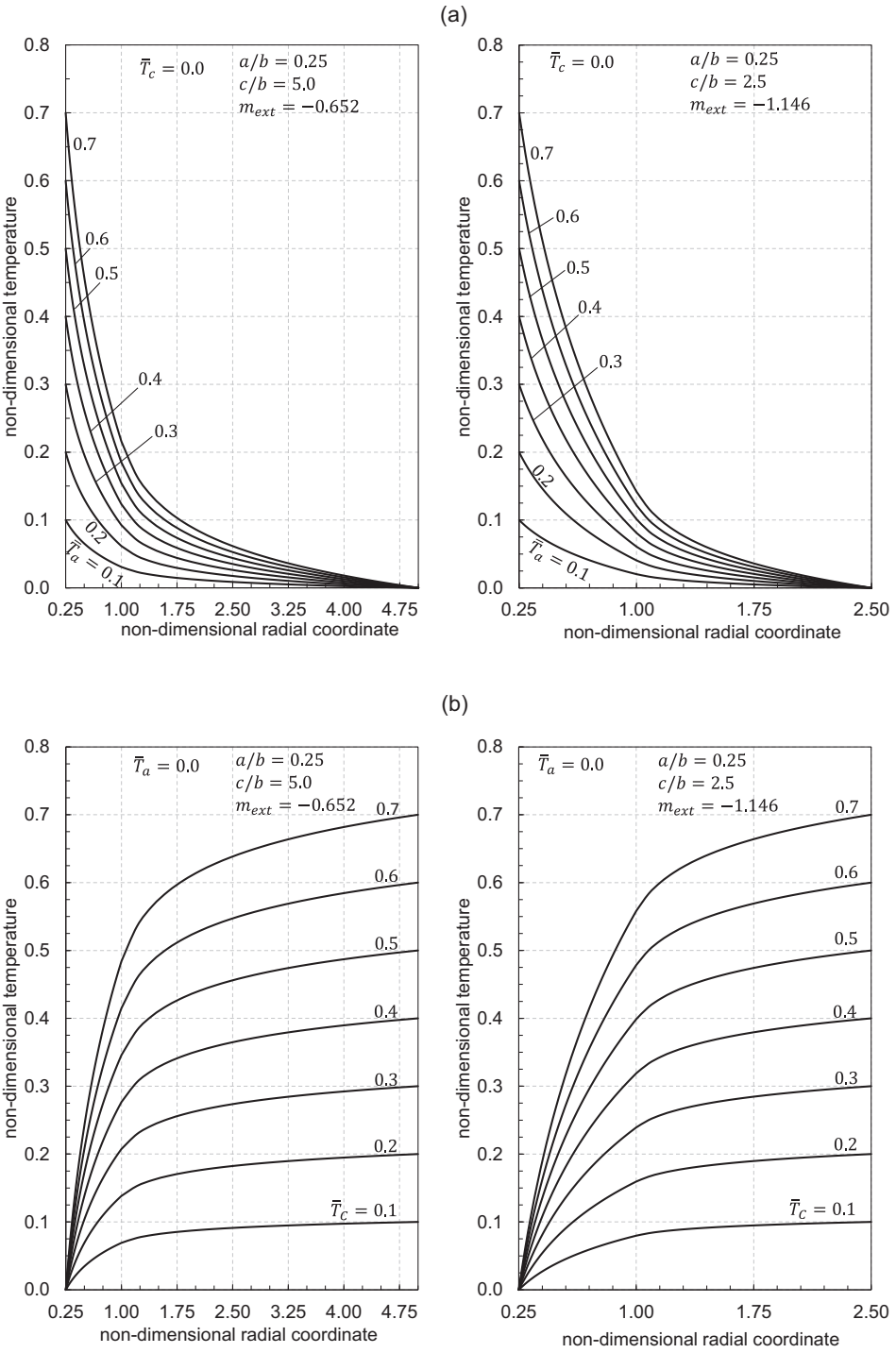


Figure 3. Examples of inhomogeneous temperature fields in shrink fits with FGM-hub; (a) heated inner surface and (b) heated outer surface.

$\Omega_{\lim(m\to 0)} = 0.19$ a homogeneous hub loses even at ambient temperature the contact with the inclusion, whereas for the FGM-hub this occurs only at $\Omega_{\lim(m=-0.652)} = 0.257$. On the other hand, as already mentioned, for $\Omega < \Omega_{\lim,FGM}$ a homogeneous hub can resist higher values of $\bar{T}_a$

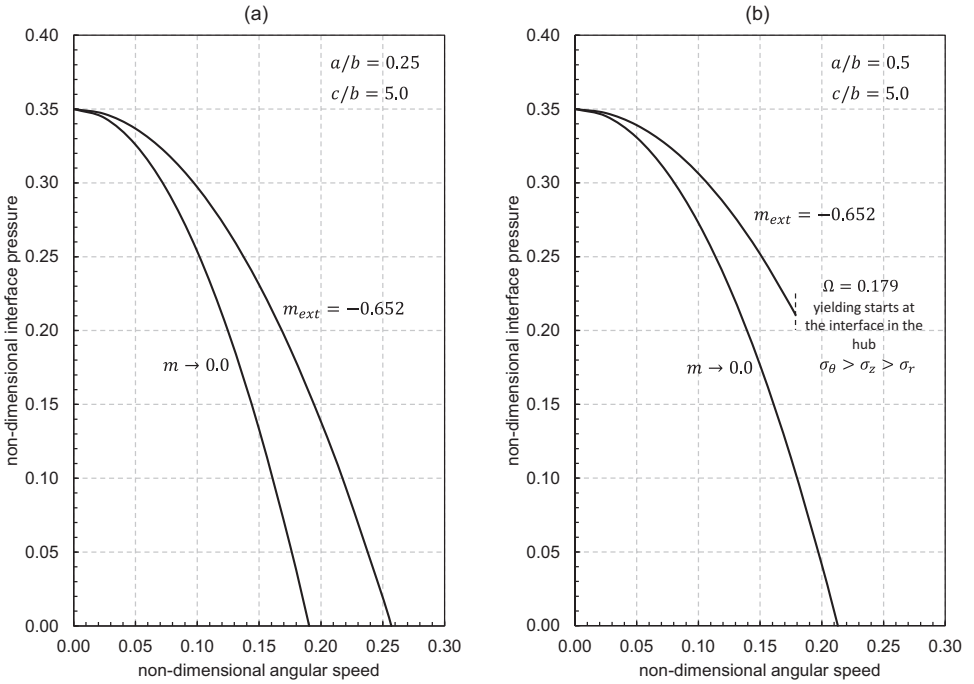


Figure 4. Evolution of the interface pressure with increasing angular speed for a shrink fit at ambient temperature with homogeneous hub ($m \to 0$) and an FGM-hub with $m = m_{ext}$, respectively. (a) Thick-walled inclusion and (b) medium-walled inclusion.

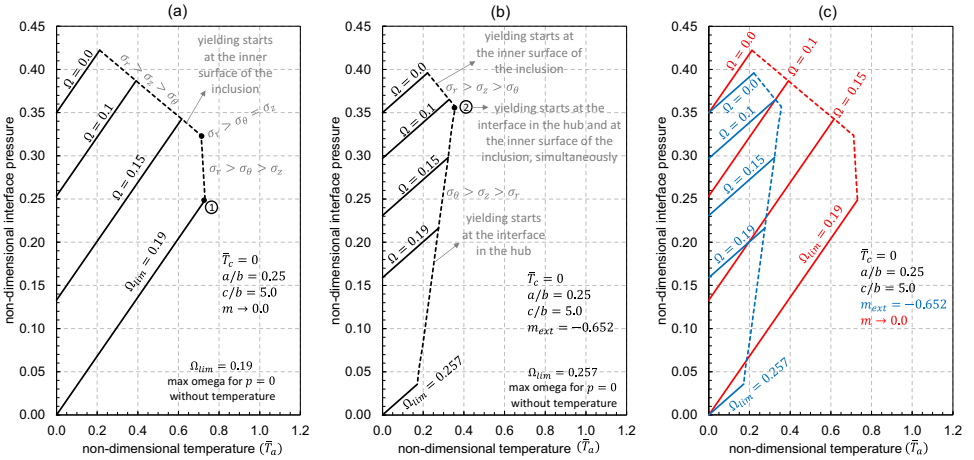


Figure 5. Interface pressure and elastic limits vs. inner surface temperature $\bar{T}_a$ at different angular speeds for a shrink fit with thick-walled inclusion ($\bar{a} = 0.25$); (a) homogeneous hub, (b) FGM-hub with $m = m_{ext}$, and (c) direct comparison of both types of hub (red lines: homogeneous hub, blue lines: FGM-hub).

without plastification, in general. Hence, with respect to the interface pressure, the FGM-hub proves superior at rotation and low inner surface temperature whereas a homogeneous steel-hub allows for higher inside temperature, albeit with noticeably worse performance at rotation.

The behavior is entirely different if the shrink fit with thick-walled inclusion is heated from the outside, see Figure 6a. As one observes, $\bar{p}$ decreases with increasing positive temperature gradient at all angular speeds, irrespective of the hub-material. Nevertheless, for all values of $\bar{T}_c > 0$ (admissible for elastic behavior) the interface pressure is higher for a rotating shrink fit with

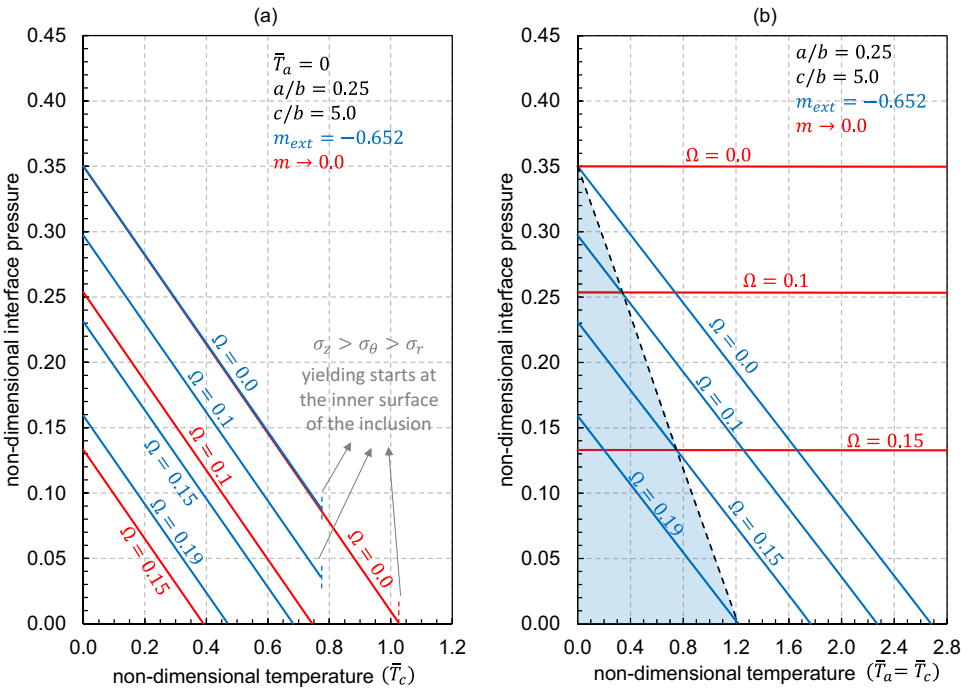


Figure 6. Interface pressure and elastic limits at different angular speeds for a shrink fit with thick-walled inclusion ($\bar{a} = 0.25$) for both a homogeneous hub (red lines) and an FGM-hub (blue lines); (a) vs. outer surface temperature $\bar{T}_c$ (the lines for $\Omega = 0.0$ are almost identical) and (b) vs. homogeneously elevated temperature.

FGM-hub than for one with homogeneous hub. Thus, in this case grading of the hub clearly proves beneficial.

From the engineering point of view, the most frequently occurring thermal load case will however be the one of—essentially—homogeneous heating. For $\bar{T}_a = \bar{T}_c$, the behavior of the shrink fit under consideration is depicted in Figure 6b. Of course, as already mentioned in the Introduction, for a homogeneous shrink fit a spatially constant elevated temperature does not influence the stress distribution. On the contrary, for the shrink fit with FGM-hub the interface pressure decreases with increasing temperature, with a however less steep gradient than in the previous case (note the different abscissa scales in Figure 6a and b). Nevertheless, using an FGM-hub may still be advantageous for moderate homogeneously elevated temperature: for operating conditions in the shaded region left of the dashed (black) line in Figure 6b the FGM-hub shows better performance, for operating conditions right of this line a homogeneous hub is recommandable (if, again, weight-reduction is not the primary assessment criterion).

As a supplement, Figure 7 presents just two examples of the stress distributions and the displacements in the shrink fit. Specifically, the case of elevated inner surface temperature is considered, and the stresses shown in Figure 7a correspond to the load condition 1 in Figure 5a for a homogeneous hub: that is, the yield limit is just reached at the inner surface of the shrink fit. As one observes, dominating stresses are the compressive circumferential and axial stresses near the inner edge of the inclusion. Moreover, in the hub all of the stresses show their extrema at the interface radius, which in case of $\bar{\sigma}_r$ is intended, of course. For comparison, in Figure 7b the stresses corresponding to load condition 2 in Figure 5b for the FGM-hub at the elastic limit are depicted. In this case, Tresca's yield criterion is fulfilled simultaneously at the inner surfaces of both the inclusion and the hub. Whereas the distributions of $\bar{\sigma}_r$ and $\bar{\sigma}_\theta$ in the inclusion are not too different from the ones in Figure 7a, the extrema of these stress components in the hub are noticeably more pronounced.

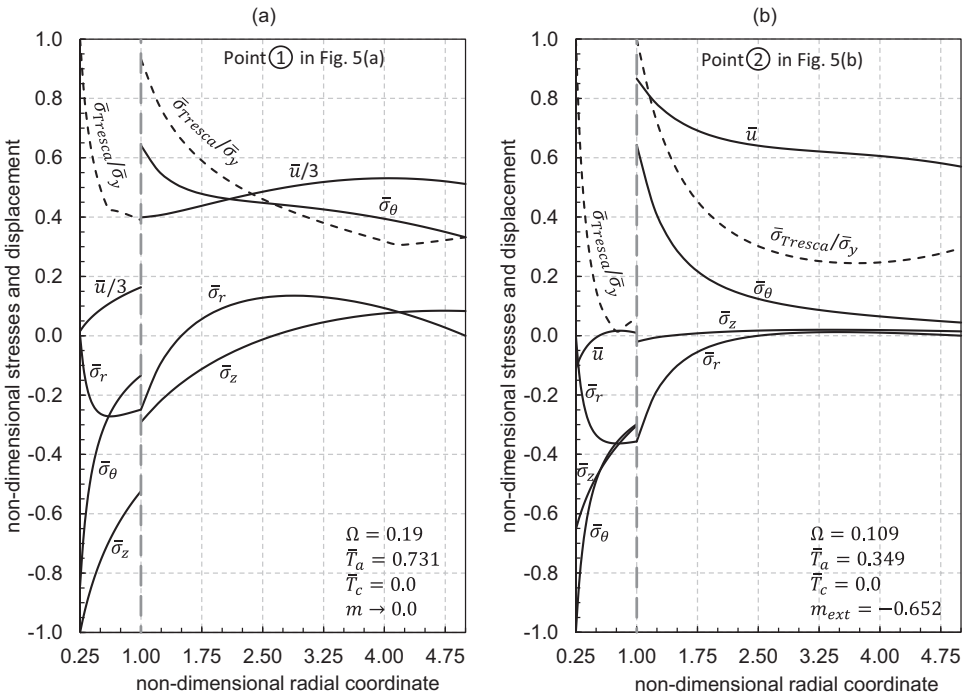


Figure 7. Distribution of stresses and displacement in a shrink fit with thick-walled inclusion ($\bar{a} = 0.25$) at elevated inner surface temperature; (a) homogeneous hub, load corresponding to point ① in Figure 5a and (b) FGM-hub, load corresponding to point ② in Figure 5b.

Next, the case of a medium-walled inclusion with $\bar{a} = 0.5$ is considered; again, an initial interface pressure of $\bar{p} = 0.35$ is presupposed. Figure 8 shows the interface pressure in an internally heated shrink fit at different angular speeds for a homogeneous hub and a maximum graded FGM-hub, respectively. For the homogeneous hub, a comparison of Figure 8a with Figure 5a reveals that $\Omega_{\lim(m\to 0)} = 0.213$ is somewhat higher for the thinner inclusion, whereas the maximum achievable interface pressure (within the elastic range) is slightly lower in this case; nevertheless, on the whole the behavior is similar. In contrast to this, comparing Figure 8b with Figure 5b, one observes that the different width of the inclusion has a noticeable qualitative effect in case of the FGM-hub: In particular, the range of loads admissible for elastic behavior is significantly smaller for $\bar{a} = 0.5$. Hence, with respect to the interface pressure, in this case a homogeneous hub is advantageous, but only at higher loads; indeed, the direct contrast of $\bar{p}(\Omega, \bar{T}_a)$ for a homogeneous hub and the FGM-hub, respectively, reveals that for small thermal loads and not too high angular speeds a graded hub still shows some benefits (Figure 8c).

On the contrary, in case of elevated outer surface temperature of the shrink fit (see Figure 9a), the dependence of the interface pressure on $\bar{T}_c$ and Ω for an inclusion with $\bar{a} = 0.5$ is qualitatively and quantitatively rather similar to the one for a thick-walled hub depicted in Figure 6a. Hence, for $\bar{T}_c > 0$ using an FGM-hub proves advantageous for almost all types of loads.

If, finally, the practically most relevant case of homogeneous heating is considered again (see Figure 9b), for $\bar{a} = 0.5$ the benefits of the FGM-hub are restricted to combinations of temperature and angular speed within the shaded region, i.e., particularly to low operating temperatures. Nevertheless, it must be emphasized once more that here only the achievable interface pressure and not the possible weight reduction by using an FGM-hub is taken into account, and that the assessment is moreover based on the prerequisite of elastic behavior of the shrink fit.

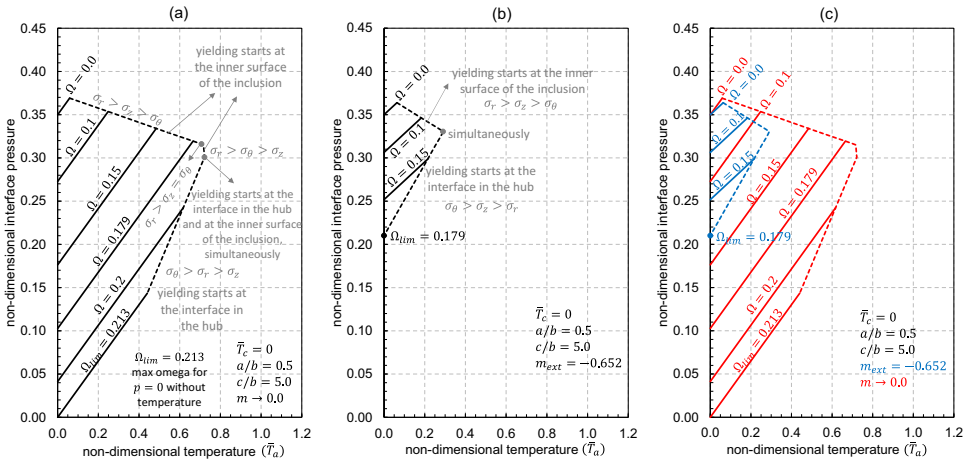


Figure 8. Interface pressure and elastic limits vs. inner surface temperature $\bar{T}_a$ at different angular speeds for a shrink fit with medium-walled inclusion ($\bar{a} = 0.5$); (a) homogeneous hub, (b) FGM-hub with $m = m_{ext}$, and (c) direct comparison of both types of hub (red lines: homogeneous hub, blue lines: FGM-hub).

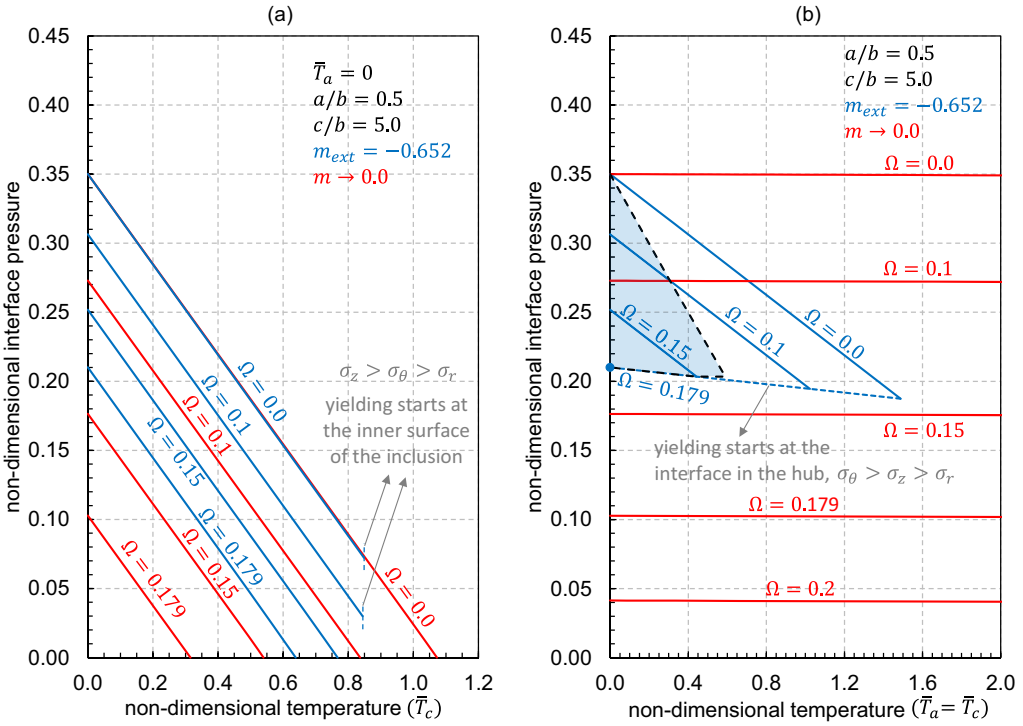


Figure 9. Interface pressure and elastic limits at different angular speeds for a shrink fit with medium-walled inclusion ($\bar{a} = 0.5$) for both a homogeneous hub (red lines) and an FGM-hub (blue lines); (a) vs. outer surface temperature $\bar{T}_c$ (the lines for $\Omega = 0.0$ are almost identical) and (b) vs. homogeneously elevated temperature.

7.2. Elastic-plastic state

Indeed, under certain conditions partial plastification of the shrink fit—particularly of the hub—may be admitted. One of these conditions is ductile behavior of the material, another one is that no dismounting of the shrink fit during its service life is intended ([16], *p.* 17); moreover, squeezing material out in the axial direction should be avoided. Roughly speaking, these conditions may

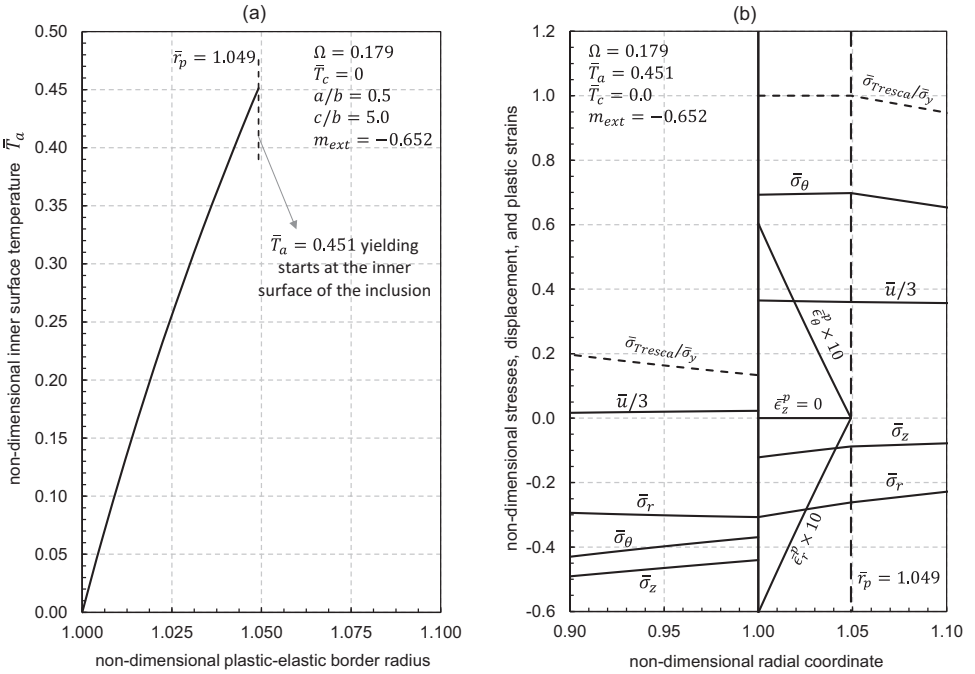


Figure 10. Shrink fit with medium-walled inclusion ($\bar{a} = 0.5$) and maximum graded FGM-hub, rotating with maximum angular speed for elastic behavior if $\bar{T} = 0$: (a) evolution of the plastic-elastic border radius with increasing values of $\bar{T}_a$ and (b) distribution of stresses, radial displacement, and plastic strains in the vicinity of the interface.

be considered sufficient for shrink fits operating at low angular speeds only and (essentially) at ambient temperature. On the contrary, as pointed out already in the Introduction, at higher angular speeds and especially also under the influence of noticeably elevated temperatures not only the variation of the interface pressure during operation but also the possible permanent stress-redistribution—which may cause a permanent decrease of the interface pressure—should be taken into account. Hence, in many cases, still an only elastic design of a shrink fit will be preferable/necessary, and such a design is in the focus of the present article.

Nevertheless, one example of plastification during operation shall be given here, too. That is, the shrink fit with medium-walled inclusion, $\bar{a} = 0.5$, and extremally graded hub is considered. Again, the results are based on $\bar{p}(\Omega = 0, \bar{T} = 0) = 0.35$, and an angular speed of $\Omega(\bar{T} = 0) = 0.179$ corresponding to the elastic limit at ambient temperature is considered (compare Figure 8b). Then, in case that the inner surface is heated, with increasing value of $\bar{T}_a$ a plastic region governed by a Tresca regime of the form given by Eq. (22) spreads in the hub. The relation between the plastic-elastic border radius $\bar{r}_p$ and $\bar{T}_a$ can be seen from Figure 10a. However, a maximum inner surface temperature of $\bar{T}_a = 0.451$ is considered, since at this temperature yielding also would start at the inner surface of the inclusion, which should be avoided, in general. The corresponding distribution of the stresses, the radial displacement, and the plastic strains in the vicinity of the interface is shown in Figure 10b: the plastic region is comparatively narrow, and therefore the effect of plastification on the stresses is not very pronounced.

As pointed out above, the influence of plastification on the interface pressure after the removal of the loads by both rotation and heating should be checked, too. In this context, a remark is appropriate. Quite generally, depending on the way of cooling of an elastic-plastic device, occurring transient temperature fields may lead to a—usually small—further expansion of the plastic region whereas in the main part thereof an elastically unloaded region spreads until the entire plastificated zone behaves elastically again (with plastic pre-deformation, of course). Typically, the

latter effect occurs very fast after the temperature has started to decrease ([30], Mack [49]), and hence in most cases it is reasonable to presume that with the onset of cooling the entire plastic zone is unloaded simultaneously. A discussion of this issue can be found, e.g., in the article by Mack and Gamer [50]. Thus, presupposing instantaneous unloading of the entire plastic region (and hence "freezing" of the plastic strains) as soon as $\bar{T}_a$ starts to decrease, the residual effect on the interface pressure can be calculated by applying the equations for elastic behavior with plastic predeformation. Here, this effect on $\bar{p}$ is small, and a permanent reduction by about 0.4% only is observed. Nevertheless, whereas this reduction is insignificant in the present case, it may be quite large in other cases and should always be checked at an elastic-plastic design of a shrink fit. However, performing this check by analytical means for a broad range of possible combinations of radii ratios, material properties, and loads would be infeasible, and one should resort to numerical techniques, in general.

8. Concluding remarks

In the above investigation, the effects of a temperature cycle on a rotating shrink fit with hollow homogeneous inclusion and power-law FGM-hub of a steel-aluminum composite have been studied, taking both homogeneous and inhomogeneous heating into account. As appropriate for a "long" device, the study has been based on a generalized plane strain condition. The focus has been not only on an elastic design, but also an example for elastic-plastic behavior was given. In the following, the most relevant results are summarized:

(i) In any case, using a steel-aluminum FGM-hub facilitates weight reduction of the shrink fit, of course. Obviously, this effect is particularly pronounced for wide hubs and large (absolute) values of the grading index; hence, the numerical results were based on such a hub.

(ii) Depending on the geometrical properties, the grading index, and the type of load, several different elastic limit cases may occur, i.e., the yield criterion may first be fulfilled at different radii.

(iii) At ambient temperature, using an FGM-hub proves significantly advantageous with respect to the evolution of the interface pressure with increasing angular speed.

(iv) In case of heating the shrink fit at the inner surface, the interface pressure increases at all angular speeds with increasing (negative) temperature gradient both for a homogeneous and an FGM-hub. Whereas a homogeneous hub allows for higher inner surface temperatures within the elastic range, for moderate temperature gradients an FGM-hub shows on the whole distinct benefits with respect to the interface pressure; this effect is particularly pronounced in case of thick-walled inclusions.

(v) If the shrink fit is heated at its outer surface, the interface pressure decreases quite generally with increasing temperature gradient. Nevertheless, an FGM-hub proves advantageous with respect to the interface pressure within the entire elastic load range, and this holds true for both thick- and medium-walled inclusions.

(vi) If the shrink fit is homogeneously heated, the elevated temperature influences the stress distribution in case of an FGM-hub only. Then, for a thick-walled inclusion there exists for not very high temperatures a range of combined rotation/heating loads where an FGM-hub is superior with respect to the interface pressure, and this superiority becomes even more pronounced at higher angular speeds. For inclusions with smaller wall-thickness the aforementioned range however diminishes, and at high operating temperatures a homogeneous hub is preferable at all angular speeds (if weight reduction is no assessment criterion).

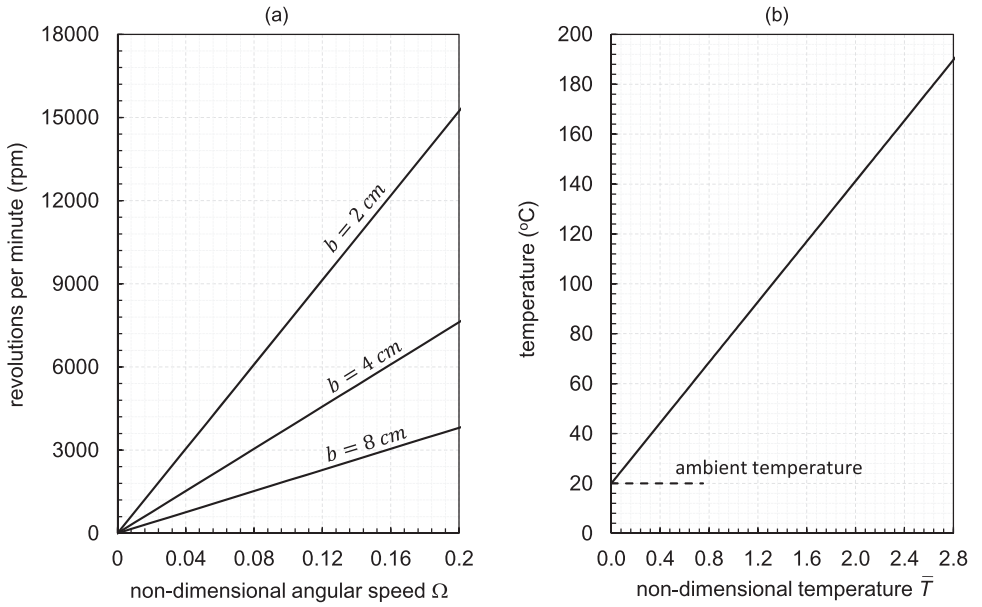


Figure 11. For a shrink fit with steel inclusion: (a) Revolutions per minute (rpm) for different interface radii vs. Ω and (b) temperature in $^{\circ}C$ vs. $\bar{T}$ (ambient temperature taken as $20^{\circ}C$).

(vii) By an example of partial plastification of an FGM-hub, caused by a temperature cycle, two issues were demonstrated. First, with increasing temperature further plastic zones may emerge somewhere in the shrink fit, which should be avoided; second, in general, by the plastification a permanent reduction of the residual interface pressure is to be expected. The latter effect may be small, but generally a significant diminution of the performance of the device cannot be excluded without sound verification at the design phase; however, in the quite general case of a heated shrink fit with FGM-hub this can be accomplished by numerical means only.

Whereas the above numerical results are based on a steel-aluminum FGM and a negative grading index, it must nevertheless be pointed out that the derived equations are universally valid. Hence, a shrink fit with a hub of some other metal-metal composite can be treated in an analogous way, provided that the basic presuppositions of the design are the same. Moreover, it shall be emphasized once more that the study could be performed by analytical means, and thus the results also may serve as benchmark solutions for future FE-studies taking more complex geometrical/material properties of the shrink fit as well as thermal conditions into account.

Appendix

To exemplify the meaning of certain non-dimensional values of angular speed Ω and temperature (difference) $\bar{T}$ in engineering, Figure 11a depicts the rpm for different interface radii and Figure 11b the temperature in $^{\circ}C$, respectively, for some steel with $E = 200\,\text{MPa}$, $\alpha = 1.65 \times 10^{-5}$ 1/K, $\rho = 7870\,\text{kg/m}^3$, and $\sigma_{ys} = 200$ MPa; the ambient temperature is taken as $20^{\circ}C$.

Acknowledgment

The authors acknowledge the TU Wien University Library for financial support through its Open Access Funding Programme.

ORCID

Eray Arslan http://orcid.org/0000-0001-9127-6149

References

[1] G. J. Nie, Z. Zhong, and R. C. Batra, "Material tailoring for functionally graded hollow cylinders and spheres," *Compos. Sci. Technol.*, vol. 71, no. 5, pp. 666–673, 2011. DOI: 10.1016/j.compscitech.2011.01.009.

[2] H. Babaei, Y. Kiani, and M. R. Eslami, "Application of two-steps perturbation technique to geometrically nonlinear analysis of long FGM cylindrical panels on elastic foundation under thermal load," *J. Therm. Stresses*, vol. 41, no. 7, pp. 847–865, 2018. DOI: 10.1080/01495739.2017.1421054.

[3] M. H. Shojaeefard, H. Saeidi Googarchin, M. Mahinzare, and M. Ghadiri, "Free vibration and critical angular velocity of a rotating variable thickness two-directional FG circular microplate," *Microsyst. Technol.*, vol. 24, no. 3, pp. 1525–1543, 2018. DOI: 10.1007/s00542-017-3557-8.

[4] B. Haghpanah Jahromi, A. Ajdari, H. Nayeb-Hashemi, and A. Vaziri, "Autofrettage of layered and functionally graded metal-ceramic composite vessels," *Compos. Struct.*, vol. 92, no. 8, pp. 1813–1822, 2010. DOI: 10.1016/j.compstruct.2010.01.019.

[5] A. Parvizi, R. Naghdabadi, and J. Arghavani, "Analysis of Al A359/SiCp functionally graded cylinder subjected to internal pressure and temperature gradient with elastic-plastic deformation," *J. Therm. Stresses*, vol. 34, no. 10, pp. 1054–1070, 2011. DOI: 10.1080/01495739.2011.605934.

[6] R. Seifi, "Exact and approximate solutions of thermoelastic stresses in functionally graded cylinders," *J. Therm. Stresses*, vol. 38, no. 10, pp. 1163–1182, 2015. DOI: 10.1080/01495739.2015.1073513.

[7] A. T. Kalali, B. Hassani, and S. Hadidi-Moud, "Elastic-plastic analysis of pressure vessels and rotating disks made of functionally graded materials using the isogeometric approach," *J. Theor. Appl. Mech.*, vol. 54, pp. 113–125, 2016. DOI: 10.15632/jtam-pl.54.1.113.

[8] J. J. Sobczak, and L. Drenchev, "Metallic functionally graded materials: A specific class of advanced composites," *J. Mater. Sci. Technol.*, vol. 29, no. 4, pp. 297–316, 2013. DOI: 10.1016/j.jmst.2013.02.006.

[9] M. M. Nemat-Alla, M. H. Ata, M. R. Bayoumi, and W. Khair-Eldeen, "Powder metallurgical fabrication and microstructural investigations of aluminum/steel functionally graded material," *Mater. Sci. Appl.*, vol. 2, pp. 1708–1718, 2011. DOI: 10.4236/msa.2011.212228.

[10] E. Arslan, and W. Mack, "Shrink fit with solid inclusion and functionally graded hub," *Compos. Struct.*, vol. 121, pp. 217–224, 2015. DOI: 10.1016/j.compstruct.2014.10.034.

[11] T. Apatay, E. Arslan, and W. Mack, "Elastic-plastic design of a rotating shrink fit with functionally graded hub," *Arch. Appl. Mech.*, vol. 87, no. 11, pp. 1829–1843, 2017. DOI: 10.1007/s00419-017-1290-5.

[12] T. Apatay, E. Arslan, and W. Mack, "Thermally loaded elastic-plastic shrink fit with FGM-Hub," *Proc. Appl. Math. Mech.*, vol. 17, no. 1, pp. 285–286, 2017. DOI: 10.1002/pamm.201710112.

[13] T. Apatay, E. Arslan, and W. Mack, "On the design of rotating elastic shrink fits with annular inclusion and functionally graded hub," *Mech. Based Des. Struct. Mach.*, vol. 47, no. 3, pp. 339–355, 2019. DOI: 10.1080/15397734.2018.1549497.

[14] J. D. Booker, and C. E. Truman, "Measuring the coefficient of friction for use in shrink-fit calculations," *Exp. Tech.*, vol. 35, no. 2, pp. 7–13, 2011. DOI: 10.1111/j.1747-1567.2009.00593.x.

[15] S. J. Chu, T. K. Jeong, and E. H. Jung, "Effect of radial interference on torque capacity of press- and shrink-fit gears," *Int. J. Automot. Technol.*, vol. 17, no. 5, pp. 763–768, 2016. DOI: 10.1007/s12239-016-0075-0.

[16] F. G. Kollmann, *Welle-Nabe-Verbindungen*. Berlin: Springer-Verlag, 1984. (In German)

[17] I. Doležel, V. Kotlan, and B. Ulrych, "Design of joint between disk and shaft based on induction shrink fit," *J. Comp. Appl. Math.*, vol. 270, pp. 52–62, 2014. DOI: 10.1016/j.cam.2014.02.023.

[18] C. Baykara, and U. Güven, "The shrink fit with plastic orthotropic hollow inclusion," *J. Reinf. Plast. Comp.*, vol. 25, no. 10, pp. 1117–1123, 2006. DOI: 10.1177/0731684406065197.

[19] N. Baldanzini, "A general formulation for designing interference-fit joints with elastic-plastic components," *J. Mech. Des.*, vol. 126, no. 4, pp. 737–743, 2004. DOI: 10.1115/1.1758247.

[20] S. Alexandrov, E. Lyamina, and Y.-R. Jeng, "A semi-analytic method for elastic/plastic shrink-fit analysis and design," *J. Strain Anal.*, vol. 50, no. 4, pp. 243–251, 2015. DOI: 10.1177/0309324715571149.

[21] A. P. Parker, and D. P. Kendall, "Residual stresses and lifetimes of tubes subjected to shrink fit prior to autofrettage," *Trans. ASME*, vol. 125, pp. 282–286, 2003. DOI: 10.1115/1.1593074.

[22] A. N. Eraslan, and T. Akis, "Yielding of two-layer shrink-fitted composite tubes subject to radial pressure," *Forsch. Ingenieurwes*, vol. 69, no. 4, pp. 187–196, 2005. DOI: 10.1007/s10010-005-0001-5.

[23] M. Sharifi, J. Arghavani, and M. R. Hematiyan, "An analytical solution for optimum design of shrink-fit multi-layer compound cylinders," *Int. J. Appl. Mech.*, vol. 4, no. 4, pp. 1250043-1-1250043-13, 2012. DOI: 10.1142/S1758825112500433.
[24] H. Lippmann, "The effect of a temperature cycle on the stress distribution in a shrink fit," *Int. J. Plast.*, vol. 8, no. 5, pp. 567–582, 1992. DOI: 10.1016/0749-6419(92)90031-7.
[25] Á. Kovács, "Thermal stresses in a shrink fit due to an inhomogeneous temperature distribution," *Acta Mech.*, vol. 105, pp. 173–187, 1994. DOI: 10.1007/BF01183950.
[26] Á. Kovács, "Residual stresses in thermally loaded shrink fits," *Period. Polytech. Mech. Eng.*, vol. 40, pp. 103–112, 1996.
[27] N. Antoni, "Contact separation and failure analysis of a rotating thermo-elastoplastic shrink-fit assembly," *Appl. Math. Model.*, vol. 37, no. 4, pp. 2352–2363, 2013. DOI: 10.1016/j.apm.2012.05.018.
[28] W. Mack, M. Plöchl, and U. Gamer, "Effects of a temperature cycle on an elastic-plastic shrink fit with solid inclusion," *J. Mech.*, vol. 16, no. 1, pp. 23–30, 2000. DOI: 10.1017/S1727719100001738.
[29] W. Mack, M. Plöchl, and U. Gamer, "Auswirkungen eines Temperaturzyklus auf einen rotierenden elastisch-plastischen Querpreßverband mit vollem Einschluß," *Z. Angew. Math. Mech.*, vol. 81, pp. S351–S352, 2001. (In German)
[30] W. Mack, and M. Plöchl, "Transient heating of a rotating elastic-plastic shrink fit," *Int. J. Eng. Sci.*, vol. 38, no. 8, pp. 921–938, 2000. DOI: 10.1016/S0020-7225(99)00064-6.
[31] V. Kotlan, P. Karban, and I. Doležel, "Induction clamping of high-revolution tools by rotation in a system of unmovable permanent magnets," *Int. J. Microstruct. Mater. Prop.*, vol. 13, pp. 99–112, 2018. DOI: 10.1504/IJMMP.2018.093311.
[32] K. Haase, "Bemessung von einfachen zylindrischen Preßverbindungen im elastischen und elastisch-plastischen Verformungszustand," *Maschinenbautechnik*, vol. 28, pp. 545–551, 1979. (In German)
[33] A. N. Eraslan, E. Arslan, and W. Mack, "The strain hardening rotating hollow shaft subject to a positive temperature gradient," *Acta Mech.*, vol. 194, no. 1–4, pp. 191–211, 2007. DOI: 10.1007/s00707-007-0456-6.
[34] E. Arslan, W. Mack, and A. N. Eraslan, "Effect of a temperature cycle on a rotating elastic-plastic shaft," *Acta Mech.*, vol. 195, no. 1–4, pp. 129–140, 2008. DOI: 10.1007/s00707-007-0549-2.
[35] Y. Ootao, and Y. Tanigawa, "Transient thermoelastic problem of a functionally graded hollow cylinder due to asymmetrical surface heating," *J. Therm. Stresses*, vol. 32, no. 12, pp. 1217–1234, 2009. DOI: 10.1080/01495730903310490.
[36] Y. Ootao, and M. Ishihara, "Transient thermoelastic analysis for a multilayered hollow cylinder with piecewise power law nonhomogeneity due to asymmetric surface heating," *Acta Mech.*, vol. 225, no. 10, pp. 2903–2922, 2014. DOI: 10.1007/s00707-014-1204-3.
[37] T. Apatay, and A. N. Eraslan, "Analyses of elastic limit heat loads in thick walled tubes subjected to periodic surface temperatures: Analytical treatment," *Arch. Mech.*, vol. 70, pp. 37–53, 2018.
[38] Y. Z. Wang, D. Liu, Q. Wang, and J. Z. Zhou, "Thermoelastic interaction in functionally graded thick hollow cylinder with temperature-dependent properties," *J. Therm. Stresses*, vol. 41, no. 4, pp. 399–417, 2018. DOI: 10.1080/01495739.2017.1422823.
[39] W. F. Chen, and D. J. Han, *Plasticity for Structural Engineers*. New York: Springer Verlag, 1988.
[40] S. Sharma, and S. Yadav, "Thermo elastic-plastic analysis of rotating functionally graded stainless steel composite cylinder under internal and external pressure using finite difference method," *Adv. Mater. Sci. Eng.*, vol. 2013, Article ID 810508. DOI: 10.1155/2013/810508.
[41] M. Z. Nejad, and P. Fatehi, "Exact elasto-plastic analysis of rotating thick-walled cylindrical pressure vessels made of functionally graded materials," *Int. J. Eng. Sci.*, vol. 86, pp. 26–43, 2015. DOI: 10.1016/j.ijengsci.2014.10.002.
[42] T. Nakamura, T. Wang, and S. Sampath, "Determination of properties of graded materials by inverse analysis and instrumented indentation," *Acta Mater.*, vol. 48, no. 17, pp. 4293–4306, 2000. DOI: 10.1016/S1359-6454(00)00217-2.
[43] M. Jabbari, S. Sohrabpour, and M. R. Eslami, "Mechanical and thermal stresses in a functionally graded hollow cylinder due to radially symmetric loads," *Int. J. Press. Vessels Piping*, vol. 79, no. 7, pp. 493–497, 2002. DOI: 10.1016/S0308-0161(02)00043-1.
[44] M. Haskul, E. Arslan, and W. Mack, "Radial heating of a thick-walled cylindrically curved FGM-panel," *ZAMM Z. Angew. Math. Mech.*, vol. 97, no. 3, pp. 309–321, 2017. DOI: 10.1002/zamm.201500310.
[45] Z. S. Shao, and G. W. Ma, "Thermo-mechanical stresses in functionally graded circular hollow cylinder with linearly increasing boundary temperature," *Compos. Struct.*, vol. 83, no. 3, pp. 259–265, 2008. DOI: 10.1016/j.compstruct.2007.04.011.
[46] U. Gamer, W. Mack, and I. Varga, "Rotating elastic-plastic solid shaft with fixed ends," *Int. J. Eng. Sci.*, vol. 35, no. 3, pp. 253–267, 1997. DOI: 10.1016/S0020-7225(96)00085-7.

[47] U. Gamer, "On the quasi-analytical solution of elastic-plastic problems with nonlinear hardening," in *Advances in Continuum Mechanics*, O. Brüller, V. Mannl, and J. Najar, Eds. Berlin: Springer Verlag, 1991, pp. 168–177.
[48] D. W. Hahn, and M. N. Özişik, *Heat Conduction*, 3rd ed. Hoboken: John Wiley and Sons, 2012.
[49] W. Mack, "Thermal assembly of an elastic-plastic hub and a solid shaft," *Arch. Appl. Mech.*, vol. 63, no. 1, pp. 42–50, 1993. DOI: 10.1007/BF00787908.
[50] W. Mack, and U. Gamer, "Zur Berechnung der Restspannungen beim Abkühlen thermisch beanspruchter elastisch-plastischer Bauteile," *Forsch. Ing.-Wes.*, vol. 54, no. 2, pp. 48–52, 1988. (In German) DOI: 10.1007/BF02563396.